Kinetics and Morphology of GaAs Etching in Aqueous CrO₃-HF Solutions

J. van de Ven and J. L. Weyher

 $Department\ of\ Solid\ State\ 3, Research\ Institute\ of\ Materials, Catholic\ University, Toernooiveld, 6525\ ED\ Nijmegen, The\\ Netherlands$

J. E. A. M. van den Meerakker and J. J. Kelly

Philips Research Laboratories, 5600 JA Eindhoven, The Netherlands

ABSTRACT

The etching of n- and p-type GaAs in aqueous CrO₃-HF solutions, both under illumination and in the dark, has been studied. On the basis of two ternary composition diagrams, three regions of different etching kinetics can be delineated. These are also regions of different surface morphology after etching. For low [HF]/[CrO₃] ratios and [HF]<10M the etching process is kinetically controlled. The etch rate depends on [HF] and is independent of [CrO₃]. High defect sensitivity is obtained in this part of the ternary diagram. For high [HF]/[CrO₃] ratios and [HF]<10M the etching reaction is limited by mass transport of CR^{VI} in solution. Defect sensitivity is poorer in these etchants. For HF concentrations above 10M, a purely chemical etching reaction becomes important and GaAs is dissolved with arsine formation. For all solutions, defects in both p- and n-type crystals are found to dissolve more slowly than the surrounding material. Kinetic and morphological results are explained in detail on the basis of a model for electroless etching.

Since the introduction of nitric acid as an etchant for GaAs by Schell (1), a large number of selective, preferential, profiling and polishing etchants has been described (2, 3). Reviews of these were given by Neels and Voigt (4), Tuck (5), Kern (6), and Stirland and Straughan (2). The latest developments in the field of defect-selective etching on GaAs are based on enhancing the contrast by illuminating the semiconductor and on slowing down etch rates by diluting the etchants (7-9). The development of new etching systems, however, is still largely a matter of trial and error. This is mainly due to the fact that, at present, very little is known about the chemistry and physics involved in the etching processes.

In recent work (10, 11) we presented a detailed model for the mechanism of GaAs dissolution in DSL etchants. DSL refers to diluted Sirtl-like etchants with the use of light. This system, which is based on CrO₃, HF, and H₂O. has already been described phenomenologically in other papers (9, 12, 13). It was shown that, for a large range of compositions, defects in n-type GaAs are revealed after removal of only some tenths of a micron from the surface. These defects include dislocations, stacking faults, microprecipitates, growth striations, and lamellar twins. The surface between the defect-related etch figures remains completely smooth. Defects can also be revealed in p-type and semi-insulating material, though the sensitivity is lower than for n-type GaAs. Because of the high defect sensitivity, the ease of handling, the stability of the solutions, the noncritical concentrations of CrO3 and HF within wide limits, and the small "memory effect" (9, 12), this system is extremely useful for delineation of defects in GaAs and other III-V compounds (14), especially in thin epitaxial layers (15). In the present paper, the morphological and kinetic aspects of GaAs etching in the DSL system are presented and discussed mainly on the basis of our model.

It should be noted that CrO₃ plays an important role as an oxidizing agent in III-V defect revealing systems. The widely used AB etchant (16) and related solutions are also based on Cr^{VI}. The use of HF in these systems gives very satisfactory results, but is not essential. It has been shown that HCl can also be used successfully, though concentrations and the concentration ratio are more critical (17).

Experimental

GaAs samples, $\{100\}$ oriented, were obtained from different manufacturers. Their specifications were: (i) n-type, Si-doped, carrier concentration of $1.2-2.8 \times 10^{18}$ cm⁻³; (ii) p-type, Zn-doped, carrier concentration of 1.3×10^{18} cm⁻³. Before use, n-type GaAs samples were anodic-

ally polished in an EDTA electrolyte (18) to remove impurities and work damage; 3-5 μ m of materials were dissolved by this procedure. The anodic oxide was left on the surface as a protective layer and was removed just before DSL etching by dipping in a diluted HCl solution. The p-type crystals received an $\rm H_2O_2/H_2SO_2/H_2O$ (by vol. 5:1:1) dip at 60°C as pretreatment; 2-3 μ m were dissolved by this treatment.

The same experiment setup was used as previously described in (9) and (10). During etching no stirring was applied. Unless otherwise stated etch rates refer to the first 30s of etching. Etch depths were determined with an Alpha step profiler (Tencor Instruments). All experiments were performed at room temperature. Chemicals, supplied by different manufacturers, were of analytical quality. Etch rates were reproducible to within 5-10%. Anomalous results, obtained with one particular batch of CrO_3 (10), are omitted from this work. Unless otherwise stated concentrations are expressed in mole/liter (M) and denoted by square brackets.

Results

Figure 1 shows the ternary diagrams with contour lines of constant etch rate for n-type GaAs in the dark (Fig. 1a) and under illumination (Fig. 1b). Etch rates for p-type GaAs, both in the dark and under illumination, were similar to those found for n-type materials in the dark.

In the composition triangles of Fig. 1 three main regions can be discerned. These are first defined and then discussed below separately. For [HF]/[CrO₃] ratios below \sim 10, the contour lines of constant etch rate run parallel to the H₂O-CrO₃ axis. This means that lines of constant etch rate are also lines of constant HF concentration. From this it follows that for solutions from this composition range, defined as region A, the etch rate depends on [HF]. For etchants with [HF]/[CrO₃] ratios above \sim 20, the contour lines run parallel to the H₂O-HF axis for a large number of solutions. In this concentration range, defined as region B, etch rates therefore depend on [CrO₃]. The transition between regions A and B occurs at [HFV[CrO₃] ratios of ~10-20. For these intermediate ratios the system must be described by mixed kinetics. The transition between the two regions is somewhat sharper for the illuminated (Fig. 1b) than for the dark (Fig. 1a) case. For solutions with high HF concentrations, deviation from the parallel behavior of the contour lines described above is evident. As will be discussed below, the linear dependence of the etch rate on [CrO₃] observed for solutions from region B, only holds for etchants with HF concentrations below 10M. Additionally, for these very concentra-

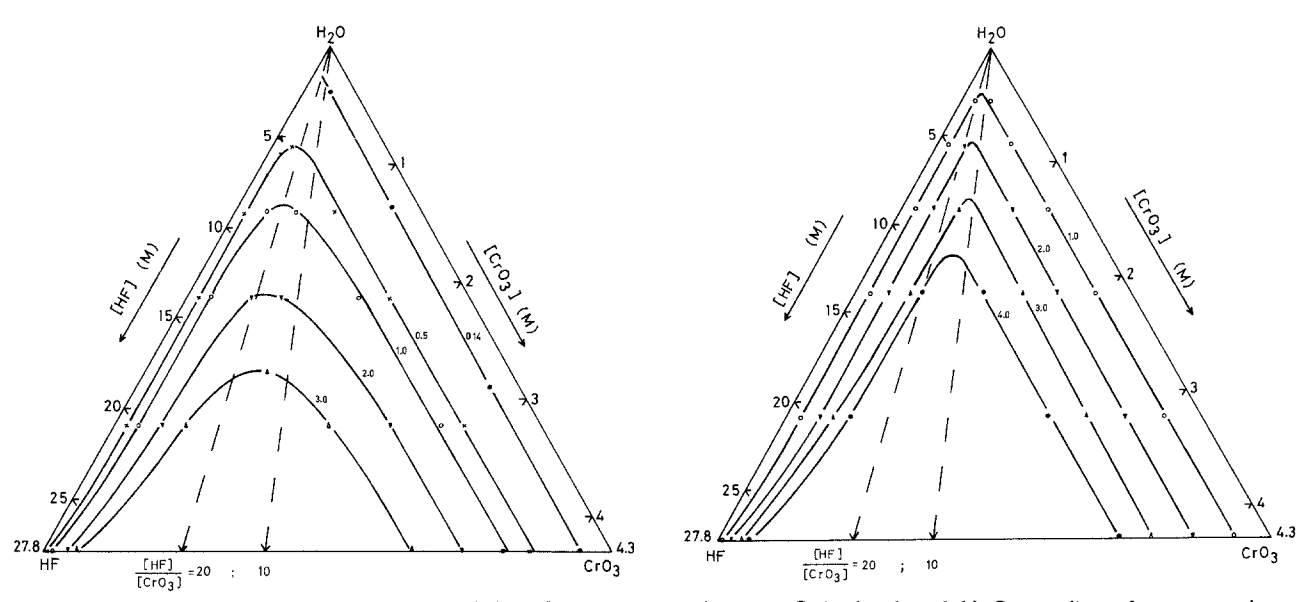


Fig. 1. Ternary composition diagrams for the HF-CrO₃-H₂O etching system for n-type GaAs. (a, above left): Contour lines of constant etch rate in the dark; (b, above right): Contour lines of constant etch rate under 150 mW/cm² He/Ne laser illumination. The numbers on the contour lines refer to etch rates in μm/min.

ted HF solutions gas bubble formation occurred during etching. Region C is therefore defined as corresponding to [HF] > 10M.

Etching kinetics in region A.—For etchants from this [HF]-controlled concentration range plots of the etch depth vs. time are linear and pass through the origin (Fig. 2). A typical etched profile is shown in the insert of Fig. 2. Etch rates of n-type GaAs in the dark and under laser illumination are plotted as a function of [HF] in Fig. 3. In the dark (curve a) the etch rate increases slowly with [HF] at low concentrations, but tends to become linear at higher [HF] values. Under illumination (curve b), a linear relationship between the GaAs dissolution rate and [HF] is found. For p-type samples a plot of the etch rate vs. [HF] is similar to that for n-type GaAs in the dark (10). The etch rate of p-type GaAs is not affected by illumination.

For all solutions from region A, the etch rate of n-type GaAs increases when light is used (Fig. 3). At increasing HF concentrations the ratio of illuminated and dark etch rates decreases markedly. This shows that at high [HF] the influence of light on the dissolution kinetics becomes small.

The photoetch rate was studied as a function of laser light intensity for some solutions from region A. A typical plot, as obtained in 1.55M HF and 1.20M CrO₃, is given in Fig. 4. In this plot the intensity is corrected for 30% light reflection losses at the air-liquid and liquid-semiconductor interfaces. This value is based on the refractive indexes of air, solution and crystal, and the absorption

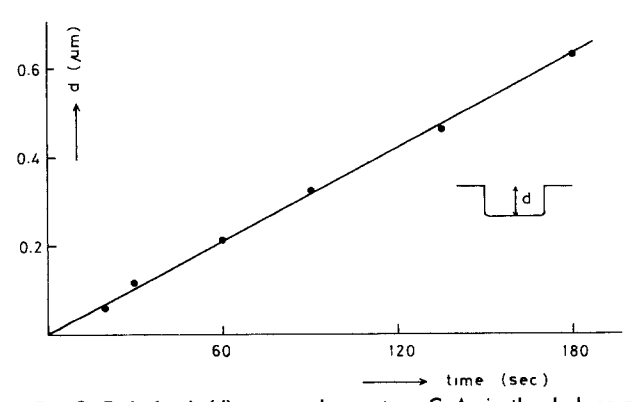


Fig. 2. Etch depth (d) measured on n-type GaAs in the dark as a function of time for an [HF]-controlled solution containing 3.10M HF and 0.96M CrO₃. In the insert a typical etch profile after 30s of etching is shown for these etchants from region A.

coefficient of GaAs at the wavelength of the light used. The curve shows that, after an initial sharp increase, the dissolution rate tends to a limiting value at high light intensities. For all experiments used to plot Fig. 1b and 3b, intensities in the saturation range were employed. From the initial (linear) slope observed in Fig. 4 the "efficiency" of illumination, defined as the number of GaAs molecules dissolved per absorbed photon, was calculated to be 0.35.

Etching kinetics in region B.—The dissolution behavior of n- and p-type crystals is the same in this [CrO₃]-controlled concentration region. A linear dependence of etch depth on time was found, but the zero-time intercept did not pass through the origin (Fig. 5). The constant steady-state etch rate can therefore deviate strongly from the rate determined after 30s of etching. For this reason it is difficult to draw quantitative conclusions regarding region B from the dissolution rates presented in Fig. 1. The steady-state etch rate, determined by measuring the etch depth for longer times (~10 min), showed a linear dependence on [CrO₃].

Illumination produced a slight increase in the etch rate of n-type GaAs. Gentle stirring or vibrating of the system, however, removed this effect. The influence of light in these cases can therefore be attributed to thermal mixing in the solution near the reacting interface. It is not a fundamental characteristic of the etching reaction itself.

At the edge of the protective wax used for etch depth determination, a "negative crown" profile was observed

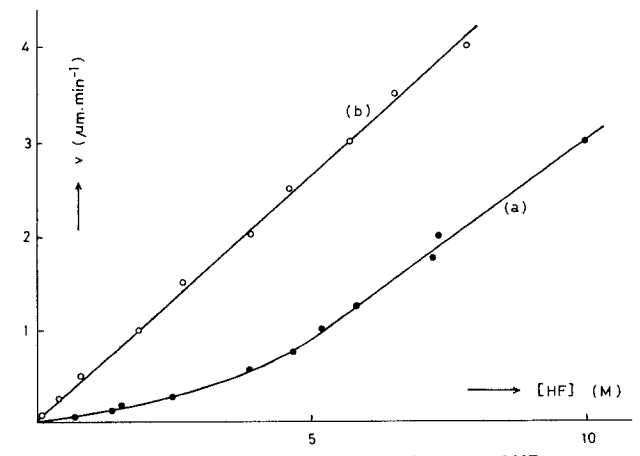


Fig. 3. Etch rates (v) of n-type GaAs as a function of HF concentration for etchants from the [HF]-controlled region of Fig. 1. Curve a is for the dark case, curve b for the illuminated case.

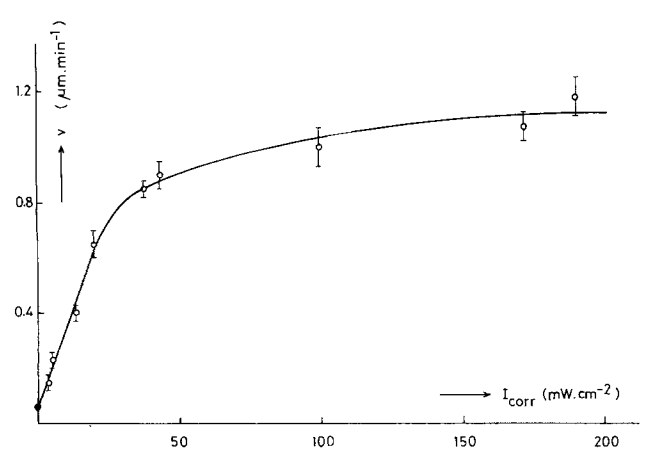


Fig. 4. Total etch rate (v) of n-type GaAs as a function of corrected laser light intensity $I_{\rm corr}$ (see text) for a solution containing 1.55M HF and 1.2M CrO $_3$.

for all solutions from region B (insert of Fig. 5). Etchants from region A did not show this effect (insert of Fig. 2).

Etching kinetics in region C.—For solutions with [HF]>10M and high [HF]/[CrO3] ratios, the etch rate exceeded the value expected on the basis of a linear [CrO₃] dependence. The difference strongly increased with increasing [HF], and could become several microns per minute for concentrations above 20M. Bubble formation in these solutions caused rough surfaces, which hampered accurate etch depth determination, and probably also introduced some stirring effects. For this reason the etch rate measurements were not very accurate and it is difficult to draw quantitative conclusions for these solutions. The "extra" etch rate discussed above causes a deviation from the parallel behavior of the etching contour lines in the ternary diagram in Fig. 1. It can be seen in Fig. 1 that this deviation is not solely a function of [HF]. In HF solutions without CrO₃, for example, no dissolution takes place. For lower CrO₃ concentrations the bending of the contour lines is also less pronounced.

To investigate whether a volatile arsenic product was present in the bubbles formed under these conditions, a fast nitrogen stream was passed over the dissolving surface. This gas was collected and analysis with induced coupled plasma (ICP) emission spectroscopy showed the presence of an arsenic-containing species. It seems very likely that arsine is formed during the dissolution process. Since this decomposes readily in the acidic and oxidizing etchant, arsine could not be detected during etching in the previous work (13). The fast nitrogen stream used in the present case, however, removed (part of) the arsine before decomposition could occur.

In Ref. (13) it was shown that the bubble formation during etching in these solutions is related to the amount of gases already dissolved in the solution before etching. The observation that this bubble formation only occurs in solutions with [HF] larger than $\sim \! 10M$, in which a volatile arsenic compound is formed at the dissolving GaAs surface, suggests that this latter reaction has a stimulating effect on bubble formation near the reacting interface. A possible explanation for this is that due to the strongly exothermic reaction of arsine in the etchant, heat is produced. This causes local gas supersaturation and consequently bubble formation.

Surface morphology after etching.—n type.—As already demonstrated in Ref. (9), etch patterns obtained on n-type GaAs vary strongly with the etchant composition. Roughly speaking, the main morphological regions that were indicated in Ref. (9) correspond to the three regions of etching kinetics in the ternary diagram. The results can be summarized as follows. In region A, with [HF][CrO₃]<10 and [HF]<10M, all kinds of defects are visible after etching (9, 12). The surface between these features remains smooth for solutions with [HF]/[CrO₃] ratios lower than ~7 (Fig. 6a). For solutions from region B and from that

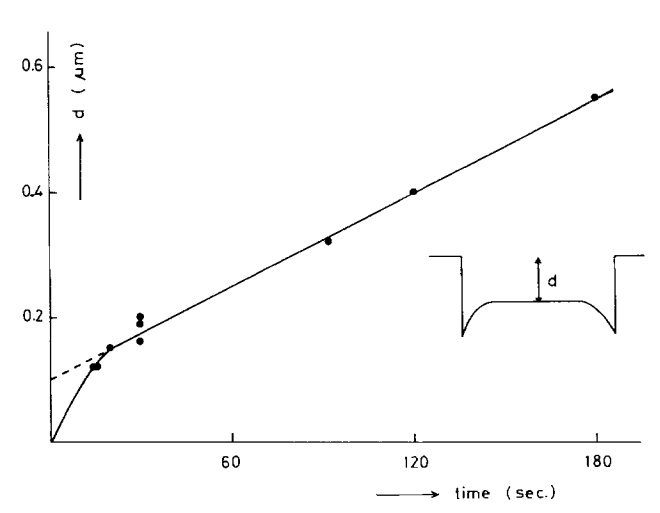


Fig. 5. Etch depth (d) measured on n-type GaAs in the dark as a function of time for a [CrO₃]-controlled solution containing 5.1M HF and 0.072M CrO₃. A typical etch profile is shown in the insert.

part of region A characterized by $[HF]/[CrO_3] > -7$, some microroughness is generally found, as well as defect structures (Fig. 6b). In concentration region C, characterized by [HF] > 10M, a so-called macroroughness is also obtained in addition to microroughness and defect features (9, 13). Large hillocks are created on the surface (Fig. 6c), which are not related to crystallographic imperfections in the semiconductor crystal. They are due to adhesion of gas bubbles to the surface, which causes local inhibition of etching.

Defects always show up as elevations or hillocks on the surface. Highest sensitivity is obtained for etchants from region A with low [HF]/[CrO₃] ratios under illumination, where removal of only a few tenths of a micron from the semiconductor surface is sufficient to reveal clearly all crystallographic imperfections. For these solutions light has a strong influence on defect sensitivity. In the dark considerably more material has to be removed to reveal the same defects (9). For solutions from region B defect sensitivity is poorer than for solutions from region A.

p-type.—The surface morphology of p-type GaAs after etching is similar to that of n-type material. Etch hillocks and ridges are formed, often with shallow depressions related to precipitates along the dislocation lines (Fig. 6d). More material has to be removed in order to reveal defects (12). For n-type GaAs under illumination removal of only 0.1-0.2 µm with a solution from region A is sufficient to reveal clearly all defects; for p-type GaAs an order of magnitude more material has to be removed in order to obtain the same resolution. Illumination has no effect on p-type defect sensitivity.

Discussion

Model.—In previous work (10, 11) we presented a model to describe the etching kinetics of GaAs in CrO₃-HF solutions. For HF concentrations lower than 10M, GaAs dissolves via an "electroless" mechanism involving two distinct electrochemical reactions: (cathodic) reduction of Cr^{VI} and (anodic) oxidative dissolution of the semiconductor. Under open-circuit (electroless) conditions, the partial currents due to these reactions must be equal. The open-circuit etch rate is related to these partial currents via Faraday's law. In this section we reconsider briefly the etching mechanism in order to analyze the kinetic and morphological results presented above.

Oxidative dissolution of GaAs occurs in several successive steps, and can be represented as follows

$$Ga: As \left(+ h^{-} \stackrel{k_1}{\rightarrow} \right) Ga: As \left([1] \right)$$

$$Ga \cdot As + h \stackrel{k_2}{\rightarrow} Ga As$$
 [2]

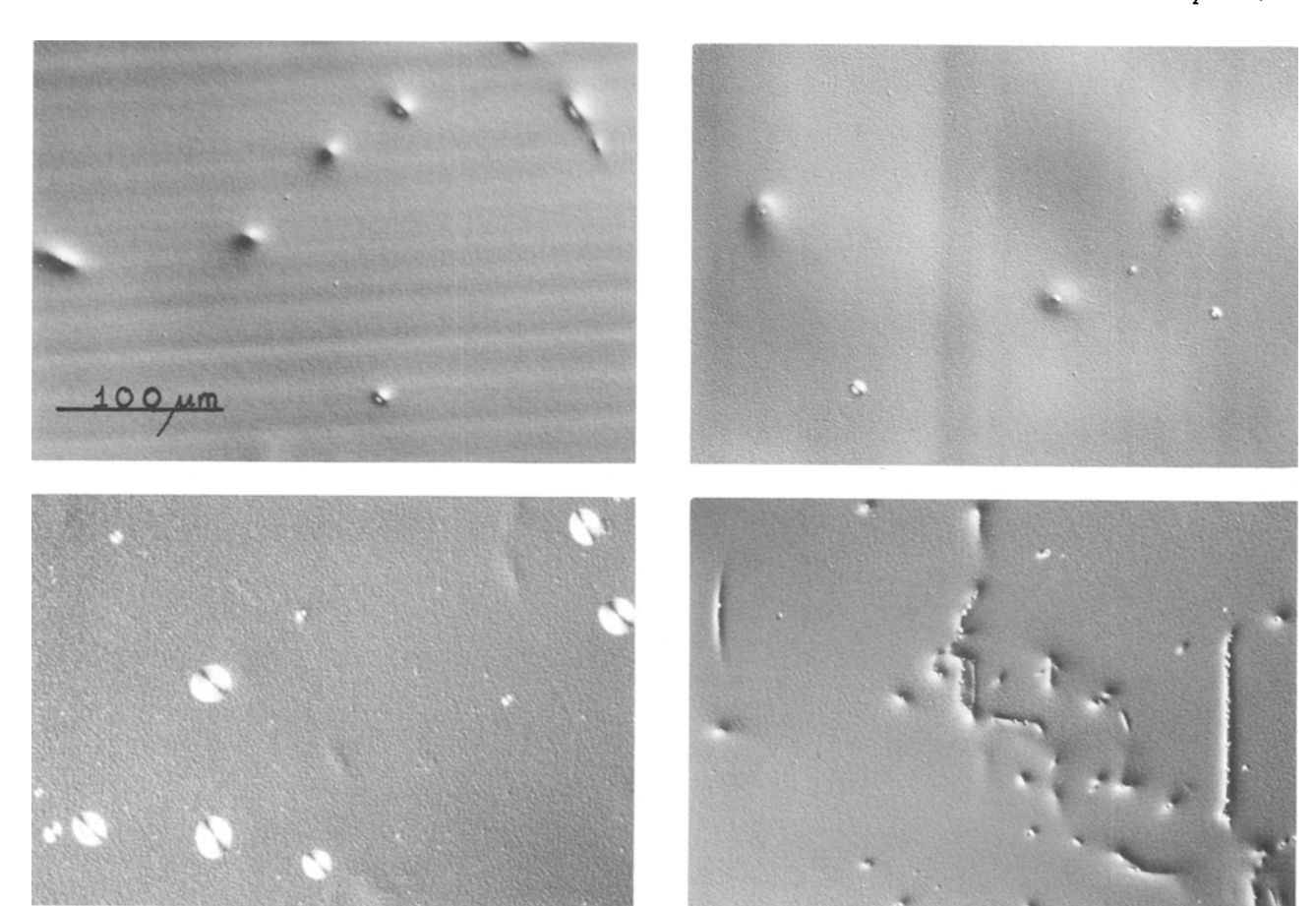


Fig. 6. Nomarski interference contrast photographs of etch patterns in GaAs illustrating regions with different surface morphology. (a, top left): Region A, n-type GaAs (defects revealed, surface flat between defects); 2.4 μm was removed in 2.3M HF, 1.8M HF, and 1.8M CrO₃ under illumination. (b, top right): Region B and solutions from region a with [HF]/[CrO₃]>~ 7, n-type GaAs (defects revealed, microroughness); 3 μm was removed in 3.7M HF, 0.29M CrO₃ under illumination. (c, bottom left): Region C, n-type GaAs (defects revealed, micro- and macroroughness); 2 μm was removed in 13.9M HF, 1.1M CrO₃ under illumination. (d, bottom right): Region A, p-type GaAs; 4 μm was removed in 4.6M HF, 0.72M CrO₃ in the dark. In order to enable a direct comparison, the etch depth was kept similar for all cases.

Ga As
$$+2X^{-} \xrightarrow{k_3}$$
 Ga As $\xrightarrow{\text{fast}}$ Ga^{III} + As^{III} [3]

In reaction [1] a hole is trapped in a GaAs surface bond. Trapping of a second hole causes a rupture of the first Ga-As bond (Eq.-[2]). Attack by a nucleophilic reagent from solution, represented by X^- , results in a rapid dissolution of the GaAs pair (Eq.-[3]). Six holes are required to dissolve one GaAs molecule (19).

If it is assumed that the trichromate ion (denoted by {Cr^{VI}-Cr^{VI}-Cr^{VI}) is the electroactive species (20), the cathodic reaction, in which holes are injected into the valence band, can be represented as follows

$$[\operatorname{Cr^{VI}-Cr^{VI}-Cr^{VI}}] \xrightarrow{k_4} [\operatorname{Cr^{III}-Cr^{VI}-Cr^{III}}]_{ads} + 6h^{\cdot}$$
 [4]

The chromium complex is reduced to a mixed valence species that forms an adsorbed blocking layer on the surface, thus preventing further hole injection and GaAs dissolution, locally. The exact nature of the hexavalent chromium species in solution is not important; the model can be readily adopted to account for other active Cr^{vi} species

The essential feature of the model involves a depassivation of the surface by reduction of the adsorbed complex with activated surface states from the GaAs oxidation process; the reduced complex is removed from the surface with the aid of HF

Ga·As + {Cr^{III}-Cr^{VI}-Cr^{III}} ads
$$\frac{k_7}{m \text{ HF}}$$
Ga As + 2 Cr^{III} + Cr^{II} + 3h⁻ [5]

In order to avoid confusion with the notation of Ref. (11), the rate constant of this reaction is denoted by k_7 . The reaction in Eq. [5] is second order in HF concentration.

The overall partial reactions can be represented as follows

$$GaAs + 6h^{-} \rightarrow Ga^{III} + As^{III}$$
 [6a]

$$\{Cr^{v_I}\text{-}Cr^{v_I}\text{-}Cr^{v_I}\} \rightarrow Cr^{II} + 2Cr^{III} + 10h^{-} \qquad [6b]$$

Etching kinetics.—From the discussion of the mechanism above it is clear that the surface coverage \ominus due to the adsorbed film must play a determining role in the etching kinetics; injection of holes from Cr^{v_1} and dissolution of GaAs via nucleophilic attack are only possible at the free surface. From Eq. [8], [9], and [14] of Ref. (11), an expression for the surface coverage of n-type and p-type GaAs in the dark at open-circuit potential can be readily obtained

$$\Theta_{\text{oc}} = \frac{5 \cdot k_4 \cdot C_{\text{ox}}}{5 \cdot k_4 \cdot C_{\text{ox}} + 2k_1 \cdot \frac{k_7}{k} \cdot C_{\text{HP}^2}}$$
[7]

The values of the various rate constants are given in Table I. $C_{\rm 0x}$ and $C_{\rm HF}$ are the concentrations of the electroactive species and HF in moles per cubic centimeter.

Table I. Rate constants for reaction steps in the GaAs dissolution process

 $k_1 = 2.5 \times 10^{-27} \, \text{mol-cm-s}^{-1} \ k_2 / k_7 = 5.5 \times 10^{-25} \, \text{mol}^2 - \text{cm}^{-3} \ k_4 = 5.5 \times 10^{-4} \, \text{cm-s}^{-1} \ A = 2.7 \times 10^8 \, \text{cm}^3 - \text{mol}^{-1}$

Note that since trichromate is considered as the hole donor, in the present case $[\text{CrO}_3] = 3 \times 10^3 \ C_{0x}$. \ominus_{oc} is obviously determined by a competition between the passivation reaction (hole injection) as given by the first term in the denominator of Eq. [7] and depassivation, which depends on reactions [1] and [5] as given in the second denominator term. From this latter term it is clear that depassivation in turn depends on the competition between reactions [2] and [5] for the GaAs activated states. The total rate of hole injection at open-circuit is described by

$$j_{\rm p} = 10k_4 C_{\rm Ox} (1 - \Theta_{\rm oc})$$
 [8]

since 10 holes are involved per electroactive species. In the steady state this rate must be, of course, equal to the rate at which the holes are consumed, *i.e.*, the dissolution rate of GaAs. Combining Eq. [7] and [8] yields the open-circuit etch rate in the dark

$$v_{\rm d} = A \frac{20 \cdot k_4 \cdot k_1 \cdot C_{\rm OX} \cdot C_{\rm HF}^2}{2 \cdot k_1 \cdot C_{\rm HF}^2 + 5 \cdot k_4 \cdot \frac{k_2}{k_7} \cdot C_{\rm OX}}$$
[9]

Here, A is a constant to express $v_{\rm d}$ in micrometers per minute.

The model predicts that for relatively low [HFV[CrO₃] ratios (depending of k_4 , k_1 , and k_2/k_7 values) the etch rate depends on the square of [HF] and is independent of [CrO₃] (Eq. [9]). This is found experimentally. In this concentration range the surface coverage due to the passivating film should be high (Eq. [7]) and the etching process should be kinetically determined by formation and dissolution of the blocking layer. This conclusion is strongly supported by electrochemical observations (10). The etching results from region A are indeed characteristic of a kinetically determined process: the etch rate of n-type GaAs can be enhanced by illumination; a steady-state etch rate is established immediately and a "negative crown" profile is not observed in Fig. 2 (see following paragraph). Etchants from region A are equivalent to the widely used AB-based systems. Since the small concentration of Ag ions in the latter etchants does not influence the etching kinetics (7), it must be concluded that the same kinetically controlled mechanism operates.

For solutions with a relatively high [HF][CrO₃] ratio, here defined as region B, Θ_{oc} should decrease to very low values (Eq. [7]) and the etch rate should depend only on the CrO₃ concentration (Eq. [9]). Hole injection by Cr^{VI}, and consequently dissolution of GaAs, proceed unhindered at the semiconductor surface. The etch rate is, in fact, limited by mass transport of Crvi in solution (10). Several observations in region B support this conclusion: initially, the etch rate is high, but it decreases to a constant value at longer etching times when a stationary diffusion boundary layer is established; stirring was found to increase etch rates; the steady-state etch rate found for longer times (without stirring) is in good agreement with the diffusion-limited reduction current of Crv1 found in electrochemical experiments (10); this steadystate etch rate is found to vary linearly with the CrO₃ concentration; and, finally, the "negative crown" profiles, observed at the resist edges (insert of Fig. 5) also indicate a mass-transport limited reaction in which more efficient supply of reactants at the resist edge locally leads to larger etch depths (21).

Using the rate constants in Table I, contour lines of constant etch rate in the dark were calculated from Eq. [9]. The results are shown in a ternary diagram and compared with experimental data (Fig. 7). The agreement is good, except for solutions from the HF-rich corner of the diagram, region C. For calculation of the etching contour lines plotted in Fig. 7, the kinetic value k_4 as given in Table I was used in all cases for the 150 reduction rate of Cr^{VI} . For solutions from region B, k_4 should be replaced by a diffusion rate constant under steady-state conditions. The experimental etch rates used to plot Fig. 1a and Fig. 7, however, were obtained after 30s of etching. Therefore, these are still determined to some extent by kinetics.

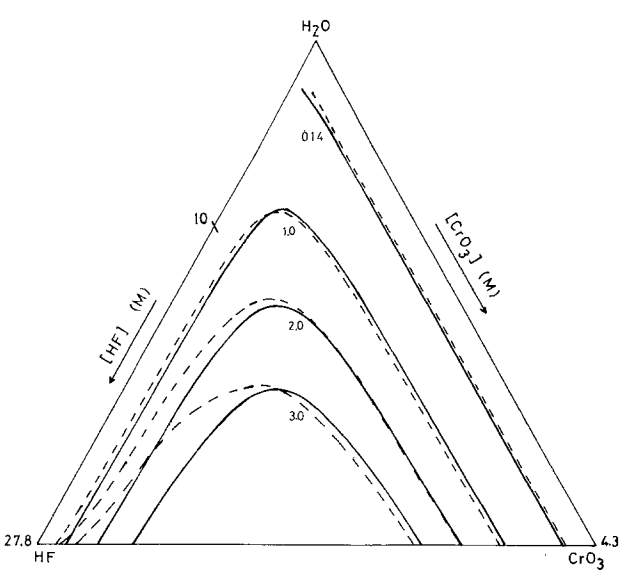


Fig. 7. Ternary composition diagram with contour lines of constant etch rate in the dark. (---) Experimental curves; (-----) curves calculated using Eq. [9] with rate constants from Table I.

For solutions containing HF concentrations above $\sim \! 10M$ (region C) it was found that etch rates are higher than expected on the basis of a reaction limited by mass transport of Cr^{v_l} . The difference increases strongly with increasing [HF]. Arsine is very likely formed under these conditions. These observations lead to the conclusion that, parallel to electroless dissolution of GaAs, a second etching mechanism operates in which GaAs is dissolved via purely chemical reaction. The equation for this reaction can be written as

$$GaAs + 3HF \longrightarrow GaF_3 + AsH_3$$
 [10]

This chemical reaction can be compared with the etching of InP in HCl solutions, during which phosphine is evolved (22). The total reaction for GaAs in CrO₃-HF solutions is, however, more complicated than that suggested in Eq. [10]. This subject is out of the scope of this paper and will not be treated further here.

Illumination of the n-type crystal during etching has a pronounced influence on the etching kinetics in solutions from region A. From the results given in Fig. 4 at low light intensities it was shown that one GaAs molecule is dissolved when three photons are absorbed. Since GaAs dissolution is in six hole process, it follows that two holes are transferred for every photon absorbed. Simple models in which photogenerated holes are used directly for GaAs oxidative dissolution cannot account for the results (11). Under electroless conditions charge neutrality must be maintained. This implies that for every hole leaving the semiconductor, an (conduction-band) electron should also be transferred to the solution. It was shown that a reduction reaction with electrons does not occur at a significant rate under open-circuit conditions (10). Therefore, the photogenerated holes and electrons must recombine and cannot contribute directly to the GaAs dissolution process. A mechanism in which GaAs surface-state intermediates participate in the recombination of the minority carriers can explain the results (11). Such a mechanism leads to a net increase in the density of activated surface states and in the rate of reaction [5], and consequently to a lowering of Θ . For n-type GaAs under electroless conditions the band bending is strong and the surface concentration of the majority carriers is very low. For p-type crystals, however, the bands are nearly flat and the high hole concentration in the light absorption region causes rapid recombination of photogenerated carriers. This explains why etching of p-type GaAs is insensitive to light.

Etching morphology.—Since defect sensitivity is highest in kinetically determined etchants, the discussion of morphology will be focused on these solutions. The defects, such as dislocations, precipitates, grain boundaries,

which are revealed by the CrO₃-HF etchants are, in most cases, crystallographically disturbed areas of the solid. These defects are revealed as hillocks or ridges on the surface. Inclusions and microprecipitates in the solid, which generally have a different composition than the matrix, may cause shallow pits on the surface during etching (9). This is thought to be due to rapid removal of such defects as a whole and will not be treated further here. In general the Gibbs free energy in regions which are stressed or in which the continuity of the lattice is broken is more positive than in the surrounding perfect crystal (23). Consequently, the change in Gibbs free energy upon dissolution, ΔG_{dis} , is more negative for defects than for the perfect surface. Working along the same lines, Frese and co-workers (24), using a bonding model of Sanderson, have shown that regions where dislocations emerge at the surface have a more negative "microscopic decomposition potential." With a simple model it is shown that decreasing the coordination number of a surface atom by one bond results in a decrease of $\Delta G_{
m dis}$ of ~140 kJ/mole. Therefore, selective corrosive attack is expected at defect areas when GaAs is etched in the dark. Consequently, enhanced dissolution of defects should lead to etch pit formation, if further general conditions required for pit formation are fulfilled (25). However, in contrast to this, hillocks or ridges are formed on all crystallographic defects during etching of n-type and p-type GaAs in CrO₃-HF solutions, both in the dark and under illumination.

In the present etching system, reduction of bond strength in the crystallographically deformed regions is expected to cause an increase in the rate constants k_1 , k_2 , and k_3 for GaAs oxidation (see Eq. [1]-[3]). Since k_7 describes charge transfer across the semiconductor/film interface, it is reasonable to assume that its value will not change significantly for defect-free or deformed material. For p- and n-type electroless etching in the dark, the dissolution rate is given by Eq. [9]. As k3 does not appear in this expression, it is not considered further. The constant k_2 involves the breaking of a Ga-As bond (Eq. [2]), and consequently a reduction of the coordination number. Therefore, crystallographic deformation is likely to have a stronger influence on k_2 than on k_1 , which only describes trapping of the first hole. Since breaking of a surface bond involves large changes in $\Delta G_{\rm dis}$ (24), a considerable increase in rate constants may be expected. In Fig. 8, the ratio of etch rates of the perfect surface and of a defect region is calculated as a function of k_2/k_7 using Eq. [9]. k_1 is, for convenience, kept constant. A strong decrease in etch rate with increasing k_1/k_7 ratio is predicted. The seemingly contradictory result, that a locally weakened bond strength causes a decrease in etch rate, results from an in-

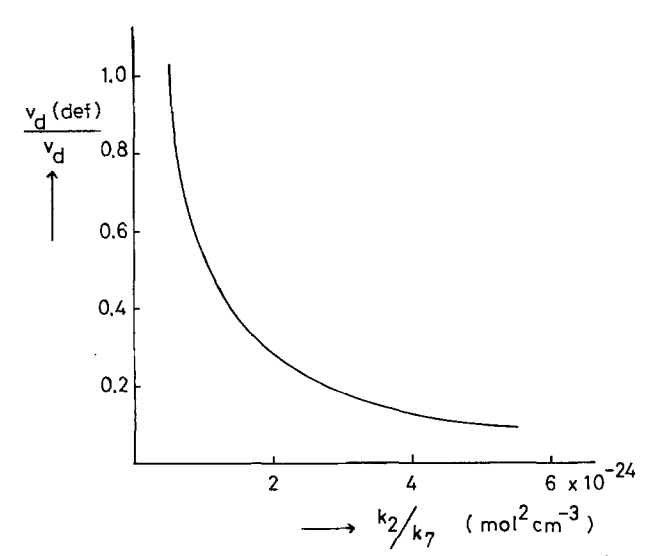


Fig. 8. Ratio of etch rates of a defect region and the perfect surface $(v_{cl}(def)/v_{cl})$ as a function of the k_{cl}/k_{τ} ratio for low [HF]/[CrO₃] ratios, calculated using Eq. [9].

creased preference of the system for reaction [2] compared to reaction [5]. Since reaction [5] ensures a depassivation of the surface, the coverage by the adsorbed layer is higher at the defect. This results in a localized decrease in etch rate and hillock formation. This behavior is somewhat analogous to that of very non-noble metals such as Al and Ti on which, partly as a result of their high corrosivity, very resistant surface films are formed which protect the material from further oxidation.

Growth striations, representing regions with different carrier concentrations, are revealed on p-type crystals by the CrO₃-HF etchants. For p-type samples with various carrier concentrations, a difference in etch rate was not found. This is in agreement with the model and Eq. [9]. However, etching of a (Zn-diffused) p/p+ profile in a DSL etchant showed preferential dissolution of the p⁻ region (26). This effect can be explained by cathodic protection of the more noble lower-doped region (Fig. 9). At the respective rest (open-circuit) potentials (V_r) of the p and p materials, the etch rates are, of course, equal. For the p material, the anodic partial current of GaAs oxidation is found at lower potentials, as is V_r . In the mixed p/p^* system the rest potential assumes an intermediate value. Consequently, this leads to cathodic protection of the region with the lower carrier concentration.

For n-type crystals, the etch rate was found to be nearly constant for a large range of carrier concentrations between $10^{16}\text{-}2 \times 10^{18}$ cm⁻³. The rest potential in CrO₃-HF solutions was found to increase with an increase in carrier concentration. Consequently, for n/n junctions a similar cathodic protection effect is expected as for p/p profiles (26). For the n-type case, however, the more highly doped region must dissolve more slowly in a mixed system. This was indeed found when etching an n-(10^{16} cm⁻³) epitaxial layer on an n-(10^{18} cm⁻²) substrate. The large sensitivity of the etchants for growth striations in n-type GaAs is accordingly explained.

The etch rate of n-type GaAs in etchants dilute in HF is relatively low. Both the etch rate and the defect sensitivity can be greatly enhanced by illumination. Defects in the solid are likely to act as additional, effective, recombination centers (27). As a consequence, the photogenerated carriers, involved in the depassivation and dissolution reactions, are efficiently removed. This may be seen in terms of a lower net generation rate at the defect, which can cause a decrease in etch rate (Fig. 4). Another important factor is that the rest potential of the crystal under illumination is significantly negative with respect

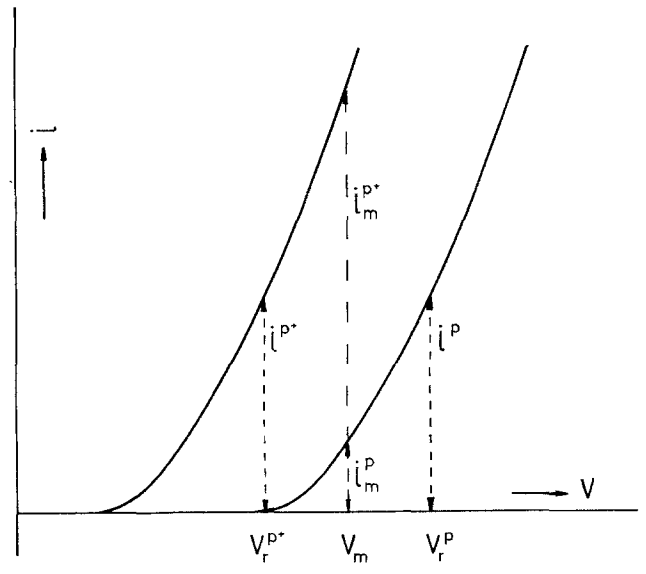


Fig. 9. Simplified current-potential plot to demonstrate the effect of cathodic protection. The anodic partial current for GaAs oxidation is shown as a function of potential for a relatively high (p') and low (p) doped sample. $V_r(p)$, $V_r(p^*)$, and V_m refer to the rest potentials for the p^- and p^- material and the p/p^- system, respectively. $i_m(p)$ and $i_m(p^*)$ refer to the anodic dissolution currents in the p/p^- system.

to V_r in the dark (10). The background "dark etch rate" is therefore greatly reduced and the photosensitivity, and thus the defect sensitivity, of the etching system is consequently enhanced.

While the latter mechanism of defect selectivity discussed above is based completely on locally enhanced recombination, the first mechanism we presented is based on lattice deformation and bond strength reduction. Therefore, differences in the shape of defects revealed after etching of p- and n-type GaAs, in the dark and under illumination, may be expected. Such effects are discussed in another paper, which deals with the interpretation of morphological features obtained after etching (12).

For kinetically-determined etchants with [HF]/[CrO₃]>~7 and [HF] lower than 10M, the etched surfaces are "microrough." Generally, for dissolution processes in highly undersaturated solutions kinetic roughening of the surface may occur (28). In the present system, however, the surface is protected by the passivating layer. This is believed to be the reason that it remains smooth during etching. Consequently, for decreasing values of the coverage Θ_{or} a "roughening transition" is expected. In Fig. 10 the surface coverage due to the film in the dark is plotted as a function of HF-concentration for [CrO₃] = 1.2M, using rate constants from Table I. For relatively low HF concentrations the surface is almost completely covered $(\Theta_{oc} \approx 1)$. For relatively high concentrations Θ_{oc} decreases to low values. The "critical" [HF]/[CrO₃] ratio of 7 corresponds to a value for \ominus_{oc} of ${\sim}0.6$ in this case. Similar results were obtained for other CrO₃ concentrations. Therefore, it is concluded that the transition from smooth to rough etched surfaces is due to a decrease in surface coverage by the passivating film.

In etchants from composition region B, the etch rate was found to be limited by mass transport of Crv1 in solution and the surface coverage \ominus_{oc} is low. As the k_2/k_7 -ratio can be considerably higher at a defect, the local surface coverage may be larger than zero (Eq. [7]). Thus, while the etch rate on the macroscopic surface is diffusion controlled, dissolution at defects may still be hindered by the passivating film. This may explain why defects are observed, though weakly, on surfaces etched in solutions from region B.

Summary

Dissolution of GaAs in CrO₃-HF solutions generally proceeds via an electroless mechanism in which the semiconductor is oxidized and CrO3 is reduced. Three main regions of etchant composition can be delineated. For [HF]/[CrO₃] ratios below \sim 10 and [H]<10M (region A), the etching process is kinetically controlled. In the dark, pand n-type dissolution kinetics are the same. The defect sensitivity for n-type GaAs is high. More material has to be removed to reveal the same defects on p-type crystals. Illumination increases both the etch rate and defect sensitivity for n-type GaAs, but does not influence p-type

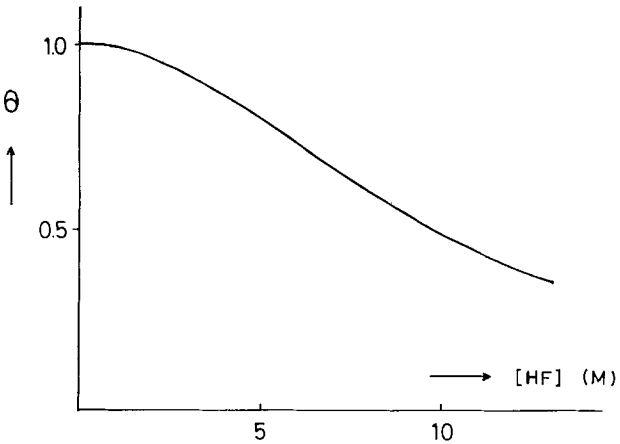


Fig. 10. Surface coverage by the passivating film, Θ_{oc} , as a function of [HF] for $[CrO_3] = 1.2M$ in the dark.

etching behavior. For [HF]/[CrO3] ratios above ~20 and [HF]<10M (region B) the etching reaction is controlled by diffusion of CrvI in the solution. The defect sensitivity is low for both n-type and p-type crystals. For solutions containing an HF-concentration above 10M (region C) a second, purely chemical, dissolution mechanism with arsine formation becomes important.

The kinetics of the electroless system were quantitatively explained, using a model involving the formation of a passivating layer which contains both Criii and Crvi species. In region A the surface coverage by the film is high. The layer can be removed by intermediates from the GaAs oxidation process, with the aid of HF. The kinetics of film formation and removal determine the etching process. In region B the coverage decreases to low values. Hôle injection by Crvi, and consequently GaAs oxidation, occur unhindered and are only limited by mass transport of Crvi.

Defects are revealed as hillocks or ridges on the surface of p- and n-type crystals, both in the dark and under illumination. Defect sensitivity on p-type GaAs and n-type GaAs in the dark can be explained by assuming a reduced bond strength at the defect. This results in a local increase in surface coverage by the passivating film and consequently a reduction in etch rate. For n-type GaAs under illumination locally enhanced recombination at defects leads to a decrease in etch rate and improved defect sensitivity. Other morphological features of the system which were explained include surface roughening and growth striations.

Acknowledgments

The authors would like to thank Dr. L. J. Giling and P. H. L. Notten for stimulating discussions. Part of this work (J. van de Ven and J. L. Weyher) was made possible by the Stichting voor Fundamenteel Onderzoek der Materie, with financial support from the Nederlandse Organisatie voor Zuiver-Wetenschappelijk Onderzoek.

Manuscript submitted June 4, 1985; revised manuscript received Dec. 2, 1985.

Catholic University assisted in meeting the publication costs of this article.

REFERENCES

H. A. Schell, Z. Metallk., 48, 158 (1957).
 D. J. Stirland and B. W. Straughan, Thin Solid Films,

- D. J. Stirland and B. W. Straugnan, 1866 1 18 239 (1981).
- J. L. Weyher and J. van de Ven, *ibid.*, **63**, 285 (1983).
 J. van de Ven, J. E. A. M. van den Meerakker, and J. J. Kelly, *This Journal*, **132**, 3020 (1985).
 J. J. Kelly, J. van de Ven, and J. E. A. M. van den Meerakker, *ibid.*, **132**, 3026 (1985).
 J. L. Weyher and J. van de Ven. In preparation.

- J. L. Weyher and J. van de Ven. In preparation.
 J. L. Weyher and W. J. P. van Enckevort, J. Cryst. Growth, 63, 292 (1983).
 J. L. Weyher and L. J. Giling, J. Appl. Phys., 58, 219
- (1985). 15. J. L. Weyher, Proc. 4th Eur. Conf. CVD, Eindhoven,
- The Netherlands, p. 273 (1983).

 16. M. S. Abrahams and C. J. Buiocchi, J. Appl. Phys., 36,
- 2855 (1965). 17. J. van de Ven, A. F. Lourens, J. L. Weyher, and L. J.
- Giling, Submitted to Chemironics.

 18. C. R. Elliott and J. C. Regnault, This Journal, 127,
- 1557 (1980).
- M. M. Faktor, T. Ambridge, C. R. Elliott, and J. C. Regnault, Curr. Topics Mater. Sci., 6, 1 (1980).
 J. P. Hoare, This Journal, 126, 190 (1979).
- 21. P. H. L. Notten, J. J. Kelly, and H. K. Kuiken, This
- Journal, To be published.

 22. P. H. L. Notten, ibid., 131, 2641 (1984).

 23. L. D. Landau and E. M. Lifshitz, Course of Theoretical Phys., 7, Pergamon, London (1959)
- K. W. Frese, Jr., M. J. Madou, and S. R. Morrison, J. Phys. Chem., 84, 3172 (1980).

25. R. B. Heimann, Crystals, 8, 173, (Springer, Berlin)

(1982). 26. J. J. Kelly, Unpublished results. 27. "Semiconductors and Semimetals," Vol. 16, R. K.

Willardson and A. C. Beer, Editors, p. 13, Academic Press, New York (1981).
28. L. A. M. J. Jetten, H. J. Human, P. Bennema, and J. P. van der Eerden, J. Cryst. Growth, 68, 503 (1984).

Reduction of Surface Stacking Faults on N-Type <100> Silicon Wafers

P. W. Koob, G. K. Fraundorf, and R. A. Craven*

Monsanto Electronic Materials Company, St. Louis, Missouri 63167

ABSTRACT

Surface stacking faults found on N-type <100> silicon wafers after a 1100°C steam oxidation have been studied using a combination of chemical etching, light microscopy, transmission electron microscopy, and energy dispersive x-ray analysis. Metal contamination (particularly Cu and Ni) present in the furnace during oxidation has been identified as a major source for these stacking faults. Results indicate that the reason N<100> wafers usually form stacking faults rather than S-pits in the presence of metal contamination is that their surfaces can more easily be contaminated with metals. Observations show that this enhanced sensitivity to metals (as compared to other wafer types and orientations) may be a result of both (i) fewer bulk defects available for intrinsic gettering, and (ii) surface orientation characteristics. N<100> surface stacking fault densities can be reduced by both furnace cleaning procedures and back-surface gettering treatments.

Defects near the polished surface of silicon wafers are of concern to device manufacturers because they are often harmful to device performance and yield. Crystallographic defects, such as surface stacking faults, play an important role in causing emitter collector shorts and piping (1). Defects such as those responsible for S-pits are thought to be harmful because, for instance, a small fraction of them grow into large surface stacking faults (2).

A variety of silicon surface defects are caused by heavy metal contamination during high temperature oxidations. For example, small copper-decorated stacking faults (3, 4), copper precipitate colonies (5), nickel nucleated inclusions (5), and rods containing Ca, S, and Fe (6) have all been observed by TEM on wafer surfaces; and all are thought to be responsible for the S-pits which develop after a preferrential chemical etch.

However, origins for the large surface stacking faults found on N-type <100>, and to a lesser extent on P-type <100> wafers, have not been fully explained. Work by Cheng and Hahn (7), which showed no relationship between surface stacking fault density and interstitial oxygen content, together with work by Murray et al. (8), which showed that surface stacking fault densities could be reduced by intrinsic gettering treatments, may point to metal contamination as a source for these defects.

The purpose of the study reported in this paper was: (i) to determine the extent to which N<100> surface stacking fault formation is caused by the presence of metal contamination in the furnace during an oxidation cycle, (ii) to identify any metal contaminant associated with a specific surface stacking fault, (iii) to establish procedures to reduce the incidence of N<100> surface stacking faults, and finally, (iv) to explore possible reasons why these large surface stacking faults are produced more abundantly on N-type <100> wafer surfaces than on P-type <111> or <100> and N<111> wafers (7).

Experimental

The 1300 silicon wafers used in the first part of this study were 3 in. diameter, medium oxygen, Czochralski grown with [100] growth direction, dislocation free, etch back, N-type (phosphorous doped), and 3-5 Ω-cm resistivity. Wafers were cut from eight crystals which had been notch coded for ingot identification. All comparisons in this study were made between wafers taken from the same location in the crystals in order to eliminate effects due to ingot position such as grown-in point defects and prior thermal history.

*Electrochemical Society Active Member.

All wafers were subjected to the following four part thermal cycle: (i) ramped heating from 800° to 1100°C in N₂, (ii) 2h pyrogenic steam oxidation at 1100°C, (iii) ramped cooling to 800°C in N2, and (iv) removal from furnace and cooling to room temperature. The wafers, following oxidation, were given a 1 min Wright etch, then were examined at 200× magnification under an optical microscope. In order to insure that the measurement of surface stacking fault number density was representative of the entire wafer surface, a total of 1.9 cm² of surface area was examined during an X-Y scan on each wafer. In addition, transmission electron microscope (TEM) specimens were prepared from non-Wright etched portions of several wafers with a wide range of surface stacking fault densities to check for the presence of other defects which may not be detected by Wright etching (e.g., S-pit defects or submicron-sized stacking faults). However, in the 42 N<100> TEM specimens examined, no defects other than the large surface stacking faults were ever found. This indicates that the Wright etch data is by itself representative of the defect population on the wafer surface.

In order to identify metallic impurities associated with individual surface stacking faults, both N-type <100> and P-type <111> wafers containing high surface stacking fault densities (>105/cm2) were examined by TEM and energy dispersive x-ray (EDX) analysis using a focused electron probe ($<20\mbox{\normalfont\AA}$). Specimens were thinned for TEM examination by either jet thinning or ion milling.

Finally, in investigating N<100> wafers' effectiveness for producing surface stacking faults, 300 low, medium, and high oxygen wafers with P- or N-type dopant and <111> or <100> orientations were examined after a variety of annealing treatments (i.e., 1100°C H₂ + O₂, 450°C, 750°C, 450°C + 775°C, 775°C + 1050°C, or 450°C + 775°C + $1050^{\circ}\text{C N}_{2}$) and Wright etch. Also, 76 TEM specimens from P<111>, P<100>, N<111> and N<100> wafers, subjected to annealing treatments (1100°C steam, 750°C N2, 1050°C N₂), were examined for bulk defect densities.

Observations

After the initial groups of wafers had been oxidized in different furnaces and analyzed for stacking fault number density, it became apparent that different furnaces produced different abundances of stacking faults (Fig. 1). Furthermore, after several more groups had been oxidized, the resulting defect counts showed that surface stacking fault density had increased for each successive